

Resonant Photon-Axion Mixing Driven by Dark Matter Oscillations

Run-Min Yao^{1, 2, *} Xiao-Jun Bi^{2, 3, †} Peng-Fei Yin^{3, ‡} and Qing-Guo Huang^{1, 2, 4, §}

¹*School of Fundamental Physics and Mathematical Sciences,
Hangzhou Institute for Advanced Study, UCAS, Hangzhou 310024, China*

²*University of Chinese Academy of Sciences, Beijing 100049, China*

³*State Key Laboratory of Particle Astrophysics, Institute of High Energy Physics, Chinese Academy of Sciences, Beijing, China*

⁴*Institute of Theoretical Physics, Chinese Academy of Sciences, Beijing 100190, China*

(Dated: January 23, 2026)

Wave propagation in periodically time-dependent media can exhibit driven mode conversion that is absent in static or adiabatic descriptions. We show that photon propagation through a coherent axion dark matter background provides a natural realization of such driven dynamics. In the presence of a magnetic field, the oscillating axion field acts as a coherent temporal drive, inducing resonant photon–axion conversion when the mismatch between their dispersion relations is compensated by integer harmonics of the axion oscillation frequency, $\Delta_\gamma - \Delta_a \approx nm_a$ with $n \in \mathbb{Z}$. This driven resonance enables efficient mixing far from the conventional level-crossing regime and disappears entirely upon time averaging, explaining why it is missed in standard treatments. The process constitutes a unitary mode-conversion phenomenon that preserves the axion dark matter number density and is distinct from parametric instabilities or axion decay. A systematic description is naturally provided by Floquet theory. We develop a general framework for photon propagation in oscillating axion backgrounds and show that the resulting resonant mixing leads to characteristic polarization signatures, with potential implications for astrophysical observations such as blazar polarization.

Introduction.— The propagation of waves in time-dependent media is a central problem across physics. When the properties of a medium vary periodically in time, wave propagation can exhibit driven mode mixing and resonant conversion phenomena that are absent in static or adiabatic descriptions. Such effects are well known in condensed matter and quantum optics [1–5], yet they have received little attention in the context of particle astrophysics.

A prominent and well-motivated realization of a coherently oscillating medium arises if dark matter (DM) [6, 7] is composed of axions [8–12] or axion-like particles [13–22]. In this case, the DM forms a classical field that oscillates at a frequency set by the axion mass over macroscopic coherence scales. Photons propagating through this background therefore experience a medium whose optical properties are intrinsically periodic in time.

Nevertheless, conventional treatments of photon–axion mixing [23–25] typically average over the axion oscillations or assume an effectively static background, thereby reducing the problem to a time-independent level-crossing or adiabatic conversion scenario. Most astrophysical studies consequently focus on birefringence [26–28] or Primakoff conversion [23, 29, 30] within quasi-static or adiabatic approximations.

In this work, we show that these assumptions miss a qualitatively new class of resonant propagation effects. Photon–axion mixing in a coherent axion DM background is intrinsically a driven process, in which the temporal periodicity of the axion field acts as a coherent driver. Resonant mode conversion occurs when the mismatch between the photon and axion dispersion relations is compensated by integer harmonics of the axion oscillation frequency, $\Delta_\gamma - \Delta_a \approx nm_a$ ($n \in \mathbb{Z}$), allowing efficient conversion even far from the conventional level-crossing condition $\Delta_\gamma \approx \Delta_a$ [31, 32]. This resonance arises purely from temporal phase matching induced by the oscillating background and does not rely on spatial inhomogeneities or finely tuned environmental profiles. The effect relies on the coherence of the axion oscillations and disappears under time averaging, explaining why it is systematically missed in standard treatments. A systematic description of such periodically driven mixing is naturally provided by Floquet theory, originally formulated in Refs. [1, 2] and reviewed in Ref. [5].

The driven resonance constitutes a unitary mode-conversion process, distinct from previously studied decay or instability phenomena [33–37], and leads to characteristic polarization signatures during propagation. While specific observational manifestations depend on environmental conditions, the underlying resonance is intrinsic to coherent axion DM and represents a previously unexplored regime of photon–axion mixing. More broadly, our results provide a general framework for wave propagation in time-dependent backgrounds and identify new resonant regimes beyond static or adiabatic descriptions.

Driven photon–axion Mixing.— The axion may couple to electromagnetism through the operator $\mathcal{L} \supset -g_{a\gamma} a F \tilde{F} / 4$, where $g_{a\gamma}$ is the photon–axion coupling with units of GeV^{-1} , a is the axion field, and F is the electromagnetic field tensor. We consider photon propagation in the presence of a magnetic field and a coherently oscillating axion background (see also Refs. [38–40] for a similar system). The axion field is treated as a classical,

homogeneous background,

$$\bar{a}(t, z) = m_a^{-1} \sqrt{2\rho_{\text{DM}}} \cos(m_a t + \varphi_a) \quad (1)$$

where m_a is the axion mass, ρ_{DM} is the DM density, and φ_a an a priori unknown phase. The axion-photon mixing equations in the presence of an external magnetic field can be reduced to a system of first-order differential equations via the WKB approximation, assuming the beam energy ω is much larger than the axion mass m_a . We consider photon propagation along the z -axis in the presence of a transverse magnetic field \mathbf{B}_T . In the linear polarization basis, the photon-axion system obeys the Schrödinger-like propagation equation,

$$i\partial_z \Psi = [\mathcal{H}_0 + \mathcal{H}_1] \Psi \quad (2)$$

where the state vector Ψ denotes the two photon polarization states and the axion field. The photon components correspond to linear polarizations oriented perpendicular and parallel to the direction of the external magnetic field. The dynamics is governed by a Hermitian mixing Hamiltonian with an explicit periodic time dependence induced by the oscillating axion background.

The static part \mathcal{H}_0 describes conventional photon-axion mixing in a magnetized medium and is given by [23–25]

$$\mathcal{H}_0 = - \begin{pmatrix} \Delta_{\perp} & 0 & 0 \\ 0 & \Delta_{\parallel} & \Delta_B \\ 0 & \Delta_B & \Delta_a \end{pmatrix}. \quad (3)$$

Throughout this work, all dispersion and mixing effects are parametrized in terms of Δ -parameters following the standard photon-axion mixing notation. Here, $\Delta_{\perp, \parallel}$ represent the photon dispersion for the two linear polarizations, accounting for both plasma effects and vacuum birefringence. In the systems considered here, vacuum QED effects are included in $\Delta_{\perp, \parallel}$ but remain subdominant to the plasma contribution, $\Delta_{\perp, \parallel} \simeq -\omega_{\text{pl}}^2/(2\omega)$. The effective plasma frequency $\omega_{\text{pl}} = \sqrt{4\pi\alpha n_e/m_e}$ with α the fine-structure constant, where n_e and m_e denote the electron number density and mass, respectively. The axion mass-induced dispersion is given by $\Delta_a = -m_a^2/(2\omega)$, while the photon-axion mixing is governed by $\Delta_B = g_{a\gamma} B_T/2$.

The axion background generates an additional, explicitly time-dependent contribution

$$\mathcal{H}_1(z) = - \begin{pmatrix} 0 & \Delta_F & 0 \\ \Delta_F^* & 0 & 0 \\ 0 & 0 & 0 \end{pmatrix}, \quad (4)$$

arising from the axion-gradient-induced birefringence, analogous to but distinct from plasma Faraday rotation, with

$$\Delta_F = ig_{a\gamma}(\partial_t \bar{a} + \partial_z \bar{a})/2. \quad (5)$$

This axion-induced Faraday term is purely imaginary, reflecting its interpretation as a rotation generator. While similar time-dependent terms have appeared in Refs. [38–40], we formalize it here as a Floquet driving parameter Δ_F (see Supplemental Material for the full derivation from the Lagrangian level). This reformulation is not merely notational; it maps the propagation problem onto a quasi-energy framework.

Crucially, the driven contribution does not commute with the static mixing Hamiltonian, $[\mathcal{H}_0, \mathcal{H}_1(z)] \neq 0$. As a result, replacing the full time-ordered evolution operator by one generated by the averaged Hamiltonian is not a controlled approximation $\langle \mathcal{T} e^{-i \int \mathcal{H}(z) dz} \rangle \neq e^{-i \int \langle \mathcal{H}(z) \rangle dz}$. In particular, time averaging projects out the nonzero Floquet sectors responsible for the driven mode mixing, thereby eliminating the effect at the level of the Hamiltonian rather than suppressing it perturbatively.

The Hamiltonian is manifestly Hermitian, and its only explicit time dependence originates from the oscillating axion background through the birefringence term,

$$\Delta_F = -i\Delta_{\text{DM}} \sin(m_a t + \varphi_a), \quad (6)$$

where $\Delta_{\text{DM}} \equiv g_{a\gamma} \sqrt{\rho_{\text{DM}}/2}$ sets the amplitude of the axion-induced drive. This term oscillates at frequency m_a and acts as a coherent temporal drive of the photon-axion system. Along the photon trajectory we adopt the eikonal approximation $t \simeq z$ (with $c = 1$), appropriate for forward-propagating waves with a well-defined carrier frequency. In this limit, the temporal oscillation of the axion background translates into a periodic modulation along the propagation direction with period $T = 2\pi/m_a$.

The resulting propagation equation describes a three-level system subject to coherent periodic driving. Rather than eliminating this time dependence, it is convenient to reallocate it by transforming to a co-rotating frame that follows the axion-induced phase modulation. This allows the driven nature of the mixing to be made explicit while preserving the quasienergy spectrum.

We therefore perform a time-dependent unitary transformation $\Psi(z) = U(z)\Phi(z)$ with $U = u \oplus 1$, where u acts on the photon subspace as

$$u(z) = \exp[-i\theta(z)\sigma_y], \quad (7)$$

with σ_y the second Pauli matrix. The rotation angle $\theta(z) = \alpha \cos \phi(z)$, with $\alpha = \Delta_{\text{DM}}/m_a$ and $\phi(z) = m_a z + \varphi_a$, is chosen such that the contribution from $U^\dagger i\partial_z U$ exactly compensates the rapidly oscillating birefringence term Δ_F . This transformation is algebraically exact and merely redistributes the periodic dependence among the Hamiltonian matrix elements.

In the following we neglect QED vacuum birefringence, assuming $|\Delta_{\perp} - \Delta_{\parallel}|/2 \ll m_a, \Delta_{\text{DM}}$. This condition ensures that the two photon polarization states remain effectively degenerate on the scale of the axion-induced modulation, so that the driven mixing dynamics

is not suppressed by polarization dephasing. We define $\Delta_\gamma \equiv (\Delta_\perp + \Delta_\parallel)/2$ as the average photon dispersion. Then the effective Hamiltonian becomes

$$\mathcal{H}'(z) = - \begin{pmatrix} \Delta_\gamma & 0 & \Delta_B \sin \theta \\ 0 & \Delta_\gamma & \Delta_B \cos \theta \\ \Delta_B \sin \theta & \Delta_B \cos \theta & \Delta_a \end{pmatrix}. \quad (8)$$

The unitary transformation leaves the physical spectrum unchanged, but renders the periodic structure of the driven photon–axion mixing explicit, providing a natural starting point for the Floquet analysis below.

The full system is a three-level Floquet problem and can be treated as such. However, in the regime $\Delta_B \ll |\Delta_\gamma - \Delta_a|$, one of the photon propagation eigenstates is far off resonance and can be adiabatically eliminated. The dynamics then reduces to two independent photon–axion subsystems, each of which can be analyzed within the rotating-wave approximation. The effective couplings are $G^{(1)} = \Delta_B \sin \theta(z)$ and $G^{(2)} = \Delta_B \cos \theta(z)$, acting as coherent time-dependent drives.

The axion-induced phase modulation is periodic, so the couplings can be expanded in a discrete set of harmonics with amplitudes controlled by Bessel functions $J_\ell(\alpha)$. Explicitly, this follows from the standard Jacobi–Anger expansion,

$$e^{i\alpha \cos \phi} = \sum_{\ell \in \mathbb{Z}} i^\ell J_\ell(\alpha) e^{i\ell\phi}. \quad (9)$$

Writing $\sin \theta$ and $\cos \theta$ in terms of $e^{\pm i\theta}$, the couplings can be decomposed into discrete Fourier harmonics,

$$G(z) = \sum_{\ell \in \mathbb{Z}} g_\ell e^{i\ell m_a z}. \quad (10)$$

Here $g_\ell^{(1)}$ ($g_\ell^{(2)}$) is nonzero only for odd (even) ℓ , reflecting the parity structure of the two photon polarizations, and the magnitude of each harmonic scales as $g_\ell \sim \Delta_B J_\ell(\alpha)$ up to phase factors.

In this co-rotating basis, the driven photon–axion system naturally acquires a Floquet structure [5]: the oscillating axion background generates a ladder of sidebands separated by integer multiples of m_a , and the periodic off-diagonal couplings mediate transitions between propagation eigenstates whose quasi-energies differ by ℓm_a .

To make this explicit, we remove the free propagation phases and move to the interaction picture by defining $\Phi = \text{diag}(e^{i\Delta_\gamma z}, e^{i\Delta_a z}) \tilde{\Phi}$. The ℓ -th Fourier component of the coupling then acquires a phase factor $e^{i\delta_\ell z}$, with detuning $\delta_\ell = \Delta_\gamma - \Delta_a - \ell m_a$. Resonant mode mixing occurs when this phase is stationary, yielding the Floquet resonance condition

$$\Delta_\gamma - \Delta_a \approx n m_a, \quad n \in \mathbb{Z}, \quad (11)$$

corresponding to vanishing detuning δ_ℓ with the identification $\ell = n$. This condition generalizes the conventional level-crossing criterion to a periodically driven

system, demonstrating that coherent photon–axion conversion can occur even far from $\Delta_\gamma = \Delta_a$. The axion background thus supplies discrete energy quanta that compensate the photon–axion dispersion mismatch, enabling coherent conversion in a regime inaccessible to static treatments.

Near a given Floquet resonance labeled by n , retaining only the corresponding Fourier component constitutes a rotating-wave approximation, valid when the nonresonant harmonics satisfy $|\delta_\ell| \gg |g_\ell|$ for $\ell \neq n$. The dynamics then reduces to a driven two-level system undergoing coherent Rabi oscillations [41, 42] with frequency

$$\Omega_R = \sqrt{|g_n|^2 + (\delta_n/2)^2}. \quad (12)$$

The photon–axion conversion probability takes the standard form

$$P_{\gamma \rightarrow a} \approx \frac{|g_n|^2}{\Omega_R^2} \sin^2(\Omega_R z). \quad (13)$$

where γ denotes the effective photon propagation eigenstate in the co-rotating basis. Resonant conversion is sustained as long as the detuning remains within $|\delta_n(z)| \lesssim 2|g_n|$, for which the peak conversion probability exceeds 50%. This regime defines the finite bandwidth of each Floquet resonance.

Several consistency limits are immediate. In the static limit $m_a \rightarrow 0$, all sidebands collapse and the system reduces exactly to conventional photon–axion mixing. For weak modulation, $\Delta_{\text{DM}} \ll m_a$, only the lowest harmonics contribute, and the driven resonance reduces to a small, single-frequency perturbation of the standard oscillation probability.

Additional derivations are provided in the Supplemental Material, where we also discuss an equivalent formulation in the circular polarization basis. In that representation, the axion background appears as a periodic modulation of the refractive indices, providing an alternative but equivalent perspective on the driven mixing. Previous studies have considered axion-induced frequency modulation or birefringence [40], but typically treat the time dependence perturbatively or average over it, thereby missing the discrete Floquet sidebands and the associated resonant mode mixing.

Finally, we stress that the driven resonance identified here—sometimes loosely termed “parametric”—corresponds to a difference-frequency Floquet resonance and is dynamically distinct from parametric instability or stimulated axion decay at $m_a \simeq 2\omega$ [33–37]. In the present case the Hamiltonian remains Hermitian, the axion dark matter number density is conserved, and the oscillating background supplies only discrete energy quanta required to compensate the photon–axion dispersion mismatch. The result is bounded, unitary mode conversion characterized by coherent Rabi oscillations.

By contrast, parametric instability requires non-Hermitian energy pumping and access to sum-frequency

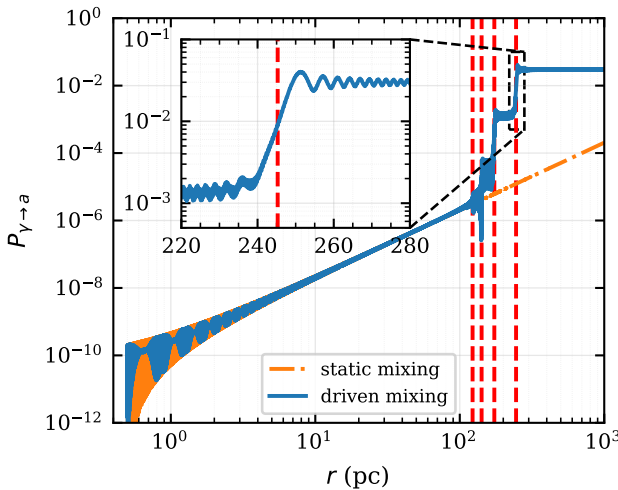


Figure 1. Photon–axion conversion probability $P_{\gamma \rightarrow a}$ along a representative blazar jet. The blue line shows the case of driven Floquet mixing with oscillating DM background, while the orange line indicates standard adiabatic conversion with static DM background. Vertical red dashed lines mark locations where $\Delta_\gamma(r) - \Delta_a \approx nm_a$.

channels, leading to exponential growth of field amplitudes. Such channels are kinematically inaccessible in the difference-frequency resonance considered here. The driven photon–axion mixing therefore realizes a stable Floquet resonance rather than an instability, as discussed further in the Supplemental Material.

Representative Propagation.— To illustrate the physical consequences of Floquet resonances, we consider photon propagation in a medium with a slowly varying dispersion $\Delta_\gamma(z)$, in the presence of a coherent axion background over the relevant length scale. This setup isolates the driven resonance mechanism without reliance on detailed source modeling.

As the photon propagates, the dispersion mismatch sweeps across the Floquet resonance condition $\Delta_\gamma(z) - \Delta_a \simeq nm_a$, activating resonant photon–axion mode conversion. Unlike conventional level-crossing scenarios, this resonance is governed by temporal phase matching and therefore does not require sharp spatial gradients or adiabaticity violation.

Figure 1 shows the resulting photon–axion conversion probability $P_{\gamma \rightarrow a}$ as a function of propagation distance for representative parameters. The driven Floquet case (blue) exhibits sharply enhanced conversion when the dispersion mismatch crosses a resonance band, whereas standard static mixing (orange) remains oscillatory and strongly suppressed. The vertical dashed lines indicate the locations where $\Delta_\gamma(z) - \Delta_a \simeq nm_a$.

The resonant region acts as a phase-matched mixing layer in which the axion oscillation continuously compensates the photon–axion dispersion mismatch. The result-

ing dynamics is directly analogous to Rabi oscillations in a coherently driven two-level system, with conversion probabilities bounded by unitarity.

We have verified that the resonance persists under moderate variations of $\Delta_\gamma(z)$ and in the presence of stochastic fluctuations, provided that the axion field remains coherent across the resonance region. The effect therefore does not rely on finely tuned environmental conditions. Further numerical details are presented in the Supplemental Material.

A direct phenomenological consequence of driven resonance crossings is the generation of polarization asymmetries between propagation modes. Repeated or stochastic crossings induce circular polarization with vanishing mean but nonzero variance. Because the axion-induced modulation enters with opposite signs for the two circular polarization states, the driven mixing mechanism is intrinsically polarization sensitive, even for initially unpolarized radiation. The variance of the circular polarization thus provides a direct observational signature of Floquet-driven photon–axion mixing.

Blazar 3C 279 as an illustration.— We validate this theoretical framework with full numerical solutions and demonstrate that the driven mixing mechanism can imprint characteristic signatures on photon polarization during propagation. As a concrete realization, we apply the formalism to optical polarimetry of the blazar 3C 279, with source-specific modeling details provided in the supplementary material.

To illustrate the potential observational impact of the mechanism, we adopt a statistical consistency criterion based on circular polarization fluctuations. Specifically, we require that the standard deviation of the axion-induced circular polarization, σ_{std} , does not exceed the characteristic observational uncertainty of a given source. For 3C 279, we take $\sigma_{\Pi_C} \approx 0.30\%$ [43]. This choice reflects the fact that, while the axion field remains phase-coherent over observational timescales, its phase φ_a is a priori unknown. As a result, the induced circular polarization does not correspond to a deterministic signal but instead manifests as a stochastic contribution with vanishing mean. In this situation, the variance provides a physically well-defined and observationally relevant measure of the effect.

Applying this criterion yields an illustrative bound on the axion–photon coupling, shown in Fig. 2 together with CAST constraints [44] for reference. For axion masses in the range $m_a \in [10^{-23}, 10^{-20}] \text{ eV}$, the resulting sensitivity reaches $g_{a\gamma} \lesssim 2 \times 10^{-11} \text{ GeV}^{-1}$ for the adopted source parameters. While the numerical level of the bound depends on the specific noise properties of 3C 279, its qualitative structure is set by the underlying driven mixing dynamics.

In particular, the banded pattern in parameter space directly reflects the discrete Floquet resonance condition associated with the periodic axion background. As m_a

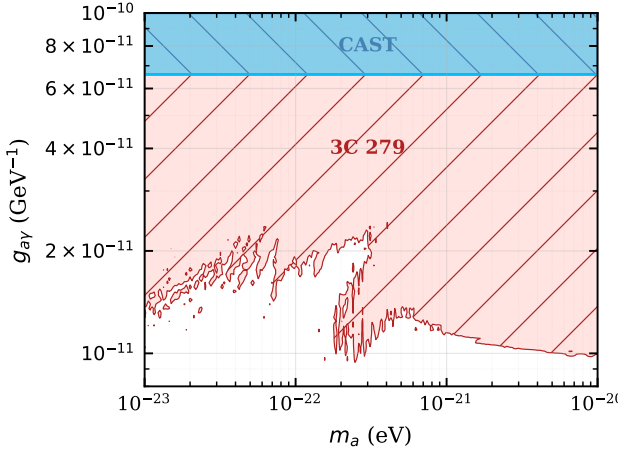


Figure 2. Illustrative bound on the axion–photon coupling $g_{a\gamma}$ derived from 3C 279 optical polarimetry. The shaded region indicates parameters excluded by the non-observation of excess circular polarization. The driven mixing mechanism gives rise to a distinctive band structure in parameter space, directly reflecting the discrete Floquet resonance condition $\Delta_\gamma - \Delta_a \approx nm_a$.

varies, the dominant contribution shifts between different resonance orders n , leading to alternating regions of enhanced and suppressed conversion. Near resonance, the driven mixing efficiently generates circular polarization, whereas between resonances the system approaches the adiabatic regime and the effect is correspondingly reduced. This characteristic structure is a direct consequence of the time-dependent Floquet driving and does not rely on fine-tuned phase alignment.

We emphasize that the bound presented here is an order-of-magnitude illustration, rather than a definitive competitive constraint. It demonstrates that the driven mixing mechanism can lead to observable, mechanism-specific polarization signatures at realistic sensitivity levels. More generally, the emergence of discrete resonance bands and stochastic circular polarization constitutes a robust phenomenological consequence of photon propagation in a coherently oscillating axion background.

Conclusions.— Wave propagation in a coherently oscillating background is intrinsically a periodically driven process. Photon propagation through axion dark matter therefore exhibits a driven resonant mode-conversion phenomenon that lies beyond the conventional static or adiabatic mixing paradigm. Resonant conversion occurs when the mismatch between photon and axion dispersion relations satisfies $\Delta_\gamma - \Delta_a \approx nm_a$, allowing coherent conversion even far from the standard level-crossing condition.

This driven resonance represents a distinct class of propagation effects. Unlike conventional resonant conversion, which is localized to regions where plasma and axion masses coincide, it arises from temporal phase matching

induced by the oscillating background and can persist over extended propagation distances. Small conversion amplitudes then accumulate coherently, leading to characteristic polarization signatures.

The effect depends on phase coherence along the propagation path. Rapidly varying environments suppress the resonance, while sufficiently smooth backgrounds allow driven conversion to operate effectively and, in some regimes, to dominate over static mixing contributions.

More generally, the framework developed here applies to wave propagation in coherently oscillating backgrounds beyond the specific axion model considered. Because the resonance relies on temporal periodicity rather than on the microscopic origin of the oscillations, analogous driven mode conversion may arise in multi-axion or other dark-sector scenarios.

Taken together, these results establish a systematic description of resonant wave propagation in time-dependent media and identify a previously overlooked driven regime of photon–axion mixing induced by coherent dark matter oscillations.

Acknowledgments.— The authors would like to thank the computing cluster of School of Fundamental Physics and Mathematical Sciences at Hangzhou Institute for Advanced Study, UCAS for providing the computational resources used in this work. This work is supported by the National Natural Science Foundation of China under Grants No. 12547110, 12475065, 12250010, 12447131, 12447105, and 12575113.

* yaorunmin@ucas.ac.cn (corresponding author)

† bixj@ihep.ac.cn

‡ yinp@ihep.ac.cn

§ huangqg@itp.ac.cn (corresponding author)

- [1] J. H. Shirley, *Physical Review* **138**, 979 (1965).
- [2] H. Sambe, *Phys. Rev. A* **7**, 2203 (1973).
- [3] S.-I. Chu and D. A. Telnov, *Physics Reports* **390**, 1 (2004).
- [4] T. Oka and H. Aoki, *Phys. Rev. B* **79**, 081406 (2009).
- [5] A. Eckardt, *Rev. Mod. Phys.* **89**, 011004 (2017), [arXiv:1606.08041 \[cond-mat.quant-gas\]](https://arxiv.org/abs/1606.08041).
- [6] F. Zwicky, *Helv. Phys. Acta* **6**, 110 (1933).
- [7] G. Bertone and T. Tait, M. P., *Nature* **562**, 51 (2018), [arXiv:1810.01668 \[astro-ph.CO\]](https://arxiv.org/abs/1810.01668).
- [8] R. D. Peccei and H. R. Quinn, *Phys. Rev. Lett.* **38**, 1440 (1977).
- [9] R. D. Peccei and H. R. Quinn, *Phys. Rev. D* **16**, 1791 (1977).
- [10] S. Weinberg, *Phys. Rev. Lett.* **40**, 223 (1978).
- [11] F. Wilczek, *Phys. Rev. Lett.* **40**, 279 (1978).
- [12] H.-Y. Cheng, *Phys. Rept.* **158**, 1 (1988).
- [13] J. Preskill, M. B. Wise, and F. Wilczek, *Phys. Lett. B* **120**, 127 (1983).
- [14] L. F. Abbott and P. Sikivie, *Phys. Lett. B* **120**, 133 (1983).
- [15] M. Dine and W. Fischler, *Phys. Lett. B* **120**, 137 (1983).

[16] A. Arvanitaki, S. Dimopoulos, S. Dubovsky, N. Kaloper, and J. March-Russell, *Phys. Rev. D* **81**, 123530 (2010), arXiv:0905.4720 [hep-th].

[17] P. W. Graham, I. G. Irastorza, S. K. Lamoreaux, A. Lindner, and K. A. van Bibber, *Ann. Rev. Nucl. Part. Sci.* **65**, 485 (2015), arXiv:1602.00039 [hep-ex].

[18] R. D. Peccei, *Lect. Notes Phys.* **741**, 3 (2008), arXiv:hep-ph/0607268.

[19] D. J. E. Marsh, *Phys. Rept.* **643**, 1 (2016), arXiv:1510.07633 [astro-ph.CO].

[20] L. Di Luzio, M. Giannotti, E. Nardi, and L. Visinelli, *Phys. Rept.* **870**, 1 (2020), arXiv:2003.01100 [hep-ph].

[21] C. B. Adams *et al.*, in *Snowmass 2021* (2022) arXiv:2203.14923 [hep-ex].

[22] C. A. J. O'Hare, *PoS COSMICWISPer*, 040 (2024), arXiv:2403.17697 [hep-ph].

[23] G. Raffelt and L. Stodolsky, *Phys. Rev. D* **37**, 1237 (1988).

[24] G. G. Raffelt, *Stars as laboratories for fundamental physics: The astrophysics of neutrinos, axions, and other weakly interacting particles* (1996).

[25] M. Kuster, G. Raffelt, and B. Beltran, eds., *Axions: Theory, cosmology, and experimental searches. Proceedings, 1st Joint ILIAS-CERN-CAST axion training, Geneva, Switzerland, November 30-December 2, 2005*, Vol. 741 (2008).

[26] S. M. Carroll, G. B. Field, and R. Jackiw, *Phys. Rev. D* **41**, 1231 (1990).

[27] S. M. Carroll, *Phys. Rev. Lett.* **81**, 3067 (1998), arXiv:astro-ph/9806099.

[28] D. Harari and P. Sikivie, *Phys. Lett. B* **289**, 67 (1992).

[29] H. Primakoff, *Phys. Rev.* **81**, 899 (1951).

[30] P. Sikivie, *Phys. Rev. Lett.* **51**, 1415 (1983), [Erratum: *Phys. Rev. Lett.* 52, 695 (1984)].

[31] M. S. Pshirkov and S. B. Popov, *J. Exp. Theor. Phys.* **108**, 384 (2009), arXiv:0711.1264 [astro-ph].

[32] A. Hook, Y. Kahn, B. R. Safdi, and Z. Sun, *Phys. Rev. Lett.* **121**, 241102 (2018), arXiv:1804.03145 [hep-ph].

[33] I. I. Tkachev, *JETP Lett.* **101**, 1 (2015), arXiv:1411.3900 [astro-ph.HE].

[34] M. P. Hertzberg and E. D. Schiappacasse, *JCAP* **11**, 004, arXiv:1805.00430 [hep-ph].

[35] A. Caputo, C. P. Garay, and S. J. Witte, *Phys. Rev. D* **98**, 083024 (2018), [Erratum: *Phys. Rev. D* 99, 089901 (2019)], arXiv:1805.08780 [astro-ph.CO].

[36] A. Caputo, M. Regis, M. Taoso, and S. J. Witte, *JCAP* **03**, 027, arXiv:1811.08436 [hep-ph].

[37] A. Arza and P. Sikivie, *Phys. Rev. Lett.* **123**, 131804 (2019), arXiv:1902.00114 [hep-ph].

[38] D. Espriu and A. Renau, *Int. J. Mod. Phys. A* **30**, 1550099 (2015), arXiv:1401.0663 [hep-ph].

[39] E. Masaki, A. Aoki, and J. Soda, *Phys. Rev. D* **101**, 043505 (2020), arXiv:1909.11470 [hep-ph].

[40] J. I. McDonald and L. B. Ventura, *Phys. Rev. D* **101**, 123503 (2020), arXiv:1911.10221 [hep-ph].

[41] L. Allen and J. H. Eberly, *Optical resonance and two-level atoms* (Courier Corporation, 2012).

[42] M. O. Scully and M. S. Zubairy, *Quantum optics* (Cambridge university press, 1997).

[43] I. Liidakis, D. Blinov, S. B. Potter, and F. M. Rieger, *Mon. Not. Roy. Astron. Soc.* **509**, L21 (2021), arXiv:2110.11434 [astro-ph.HE].

[44] V. Anastassopoulos *et al.* (CAST), *Nature Phys.* **13**, 584 (2017), arXiv:1705.02290 [hep-ex].

[45] K. M. A., A. C. Gupta, J. Fan, N. Sahakyan, C. M. Raiteri, L. Cui, A. Lahteenmaki, M. Gurwell, M. Tornikoski, and M. Villata, *Astrophys. J.* **989**, 125 (2025), arXiv:2507.03913 [astro-ph.HE].

[46] J. F. Navarro, C. S. Frenk, and S. D. M. White, *Astrophys. J.* **462**, 563 (1996), arXiv:astro-ph/9508025.

[47] H.-Y. Schive, T. Chiueh, and T. Broadhurst, *Nature Phys.* **10**, 496 (2014), arXiv:1406.6586 [astro-ph.GA].

[48] L. Ferrarese, *Astrophys. J.* **578**, 90 (2002), arXiv:astro-ph/0203469.

[49] H.-Y. Schive, M.-H. Liao, T.-P. Woo, S.-K. Wong, T. Chiueh, T. Broadhurst, and W. Y. P. Hwang, *Phys. Rev. Lett.* **113**, 261302 (2014), arXiv:1407.7762 [astro-ph.GA].

[50] A. A. Dutton and A. V. Macciò, *Mon. Not. Roy. Astron. Soc.* **441**, 3359 (2014), arXiv:1402.7073 [astro-ph.CO].

Supplementary Material for Resonant photon–axion Mixing Driven by Dark Matter Oscillations

Run-Min Yao, Xiao-Jun Bi, Peng-Fei Yin, and Qing-Guo Huang

This Supplementary Material (SM) contains additional calculation and derivation in support of the results presented in this work. First, we give a full derivation of the Hamiltonian presented in the main text. Then, we present additional details regarding the derivation of the two-level systems. Next, we discuss the relation between our work and parametric instability. Finally, we present a numerical analysis and apply the formalism to the relativistic jet of blazar 3C 279.

PHOTON–AXION CONVERSION IN AN AXION BACKGROUND

In this section, we provide the step-by-step derivation of the Hamiltonian presented in the main text.

The Lagrangian for the photon field A_μ and axion field a can be written as

$$\mathcal{L} = -\frac{1}{4}F_{\mu\nu}F^{\mu\nu} - A_\mu j^\mu + \frac{1}{2}(\partial_\mu a)^2 - \frac{1}{2}m_a^2a^2 - \frac{1}{4}g_{a\gamma}aF_{\mu\nu}\tilde{F}^{\mu\nu}, \quad (\text{S1})$$

where $F_{\mu\nu}$ and $\tilde{F}^{\mu\nu}$ denote the electromagnetic field tensor and its dual tensor, respectively, $j^\mu = (\rho, \mathbf{J})$ is the electromagnetic current density, and $g_{a\gamma}$ is the axion–photon coupling. Adopting the temporal gauge $A_0 = A^0 = 0$ and fixing the residual gauge freedom by imposing the Coulomb (radiation) gauge $\nabla \cdot \mathbf{A} = 0$, the equations of motion are:

$$\partial_t^2 \mathbf{A} - \nabla^2 \mathbf{A} = \mathbf{J} + g_{a\gamma}\partial_t a \nabla \times \mathbf{A} - g_{a\gamma}\nabla a \times \partial_t \mathbf{A}, \quad (\text{S2})$$

$$-\nabla \cdot \partial_t \mathbf{A} = \rho - g_{a\gamma}\nabla a \cdot (\nabla \times \mathbf{A}), \quad (\text{S3})$$

$$\partial_t^2 a - \nabla^2 a + m_a^2 a = -g_{a\gamma}\partial_t \mathbf{A} \cdot (\nabla \times \mathbf{A}). \quad (\text{S4})$$

For a weakly magnetized cold plasma, the dielectric tensor is isotropic, $\epsilon = (1 - \frac{\omega_{\text{pl}}^2}{\omega^2})\mathbb{I}$, where $\omega_{\text{pl}} = \sqrt{4\pi\alpha n_e/m_e}$ is the plasma frequency and ω is the energy of the photon–axion system. Here, α is the fine-structure constant, n_e and m_e denote the electron number density and mass, respectively. In the radiation gauge, longitudinal plasma oscillations decouple from the propagating electromagnetic modes. In Fourier space, the induced plasma current therefore contributes an isotropic dispersion term $\mathbf{J}_{\text{ind}}(\omega) = -\omega^2(\mathbb{I} - \epsilon)\mathbf{A}(\omega) = -\omega_{\text{pl}}^2\mathbf{A}(\omega)$ to both photon polarizations, which can be absorbed into an effective photon mass.

We apply the linearized perturbation to the equation and write the fields into background and perturbation

$$\mathbf{A} = \bar{\mathbf{A}} + \delta\mathbf{A}, \quad a = \bar{a} + \delta a, \quad (\text{S5})$$

where \bar{a} and $\bar{\mathbf{B}} = \nabla \times \bar{\mathbf{A}}$ are the background axion and magnetic fields. The perturbations satisfy the equations of motion:

$$\partial_t^2 \delta\mathbf{A} - \nabla^2 \delta\mathbf{A} + \omega_{\text{pl}}^2 \delta\mathbf{A} = g_{a\gamma} \bar{\mathbf{B}} \partial_t \delta a + g_{a\gamma} \partial_t \bar{a} \nabla \times \delta\mathbf{A} - g_{a\gamma} \nabla \bar{a} \times \partial_t \delta\mathbf{A}, \quad (\text{S6})$$

$$-\nabla \cdot \partial_t \delta\mathbf{A} = \delta\rho - g_{a\gamma} \nabla \bar{a} \cdot (\nabla \times \delta\mathbf{A}) - g_{a\gamma} \nabla \delta a \cdot \bar{\mathbf{B}}, \quad (\text{S7})$$

$$\partial_t^2 \delta a - \nabla^2 \delta a + m_a^2 \delta a = -g_{a\gamma} \bar{\mathbf{B}} \cdot \partial_t \delta\mathbf{A}. \quad (\text{S8})$$

For a magnetic field perpendicular to the photon propagation direction and an axion gradient parallel to it, the source terms in Eq.(S7) vanish. The last two terms in Eq. (S6) characterize the birefringence effect induced by the axion DM. The first terms on the RHS of Eq. (S6) and Eq. (S8) reflect the axion–photon couplings. In conventional analysis regarding the photon–axion conversion, the variation of the axion DM is neglected.

We choose the direction of the wave vector $\hat{\mathbf{k}}$ along the z -axis and adopt the plane-wave Ansatz

$$\delta\mathbf{A} = -i\tilde{\mathbf{A}}(z)e^{-i\omega t}, \quad \delta a = \tilde{a}(z)e^{-i\omega t}, \quad (\text{S9})$$

where $\delta\mathbf{A}$ includes an additional factor of $-i$ compared to δa . This choice ensure that the axion–photon coupling terms in the mixing matrix remain real, consistent with the standard form of the equations of motion found in most literature. Subsequently, we derive

$$(\partial_z^2 + \omega^2 - \omega_{\text{pl}}^2)\tilde{\mathbf{A}} = -g_{a\gamma} \bar{\mathbf{B}} \omega \tilde{a} - g_{a\gamma}(\partial_t \bar{a} \partial_z + i\omega \partial_z \bar{a})(\hat{z} \times \tilde{\mathbf{A}}), \quad (\text{S10})$$

$$(\partial_z^2 + \omega^2 - m_a^2)\tilde{a} = -g_{a\gamma} \bar{\mathbf{B}} \omega \tilde{\mathbf{A}}. \quad (\text{S11})$$

The equations can be rearranged as

$$(\partial_z^2 + \omega^2 + 2\omega\mathcal{M})\psi = 0, \quad (\text{S12})$$

where $\psi = (\tilde{A}_\perp, \tilde{A}_\parallel, \tilde{a})$, and \tilde{A}_\perp and \tilde{A}_\parallel are the amplitudes for perpendicular and parallel polarization modes, respectively. The mixing matrix is

$$\mathcal{M}(z) = \begin{pmatrix} \Delta_\perp & \Delta_F & 0 \\ \Delta_F^* & \Delta_\parallel & \Delta_B \\ 0 & \Delta_B & \Delta_a \end{pmatrix}. \quad (\text{S13})$$

Here, $\Delta_{\perp,\parallel}$ represent the photon dispersion for the two linear polarizations, accounting for both plasma effects and vacuum birefringence. In the systems considered here, vacuum QED effects are included in $\Delta_{\perp,\parallel}$ but remain subdominant to the plasma contribution, $\Delta_{\perp,\parallel} \simeq -\omega_{\text{pl}}^2/(2\omega)$. The axion mass-induced dispersion is given by $\Delta_a = -m_a^2/(2\omega)$, while the photon–axion mixing is governed by $\Delta_B = g_{a\gamma}B_T/2$ with the transverse magnetic field B_T . The Δ_F term originates from the axion-gradient-induced birefringence and is formally analogous to the Faraday rotation term. Explicitly, it is given by

$$\Delta_F \equiv \frac{g_{a\gamma}}{2\omega}(\partial_t \bar{a} \partial_z + i\omega \partial_z \bar{a}) \quad (\text{S14})$$

where the operator ∂_z in the first term acts on the photon field. Within the WKB approximation, $-i\partial_z\psi \approx \omega\psi$, the operator ∂_z acting on ψ can be replaced by $i\omega$, yielding

$$\Delta_F = \frac{i}{2}g_{a\gamma}(\partial_t \bar{a} + \partial_z \bar{a}). \quad (\text{S15})$$

The second-order equations of motion can be expressed in first-order form

$$(i\partial_z + \omega + \mathcal{M})\psi = 0. \quad (\text{S16})$$

In the derivation above, we have neglected the absorption effects of photons, the contribution of the cosmic microwave background’s energy density to the dispersion relation, and the QED vacuum birefringence effect.

Assuming a small DM virial velocity $v_{\text{DM}} \ll 1$, we model the background field as

$$\bar{a}(t, z) = m_a^{-1} \sqrt{2\rho_{\text{DM}}} \cos(m_a t + \varphi_a), \quad (\text{S17})$$

where ρ_{DM} is the DM density and φ_a is the phase of the axion background. This leads to an oscillating birefringence term:

$$\Delta_F = -i\Delta_{\text{DM}} \sin(m_a t + \varphi'_a), \quad (\text{S18})$$

where the amplitude is $\Delta_{\text{DM}} \equiv g_{a\gamma} \sqrt{(1 + \mathcal{F}^2)\rho_{\text{DM}}/2}$ and the phase is $\varphi'_a = \varphi_a + \arctan \mathcal{F}$. The factor $\mathcal{F}(z) = m_a^{-1} d \ln \rho_{\text{DM}} / dz$ can be used to describe possible corrections from spatial DM gradients, but will be neglected in the following. For fuzzy DM, $\mathcal{F}(z)$ is less than the virial velocity of DM. Along the photon trajectory we take the eikonal propagation approximation $t \simeq z$ (with $c = 1$).

EFFECTIVE TWO-LEVEL SYSTEMS

Applying $\psi(z) = e^{i\omega z}\Psi(z)$, the reduced Schrödinger-like equation can be written as

$$i \frac{d}{dz} \Psi(z) = \mathcal{H}(z) \Psi(z), \quad \mathcal{H}(z) = -\mathcal{M}(z), \quad (\text{S19})$$

where \mathcal{M} is the mixing matrix including the oscillating birefringence term. To solve the dynamics analytically, we perform a time-dependent unitary transformation $\Psi(z) = U(z)\Phi(z)$ to eliminate the rapid oscillations in the photon sub-block. The effective Hamiltonian becomes

$$\mathcal{H}'(z) = U^\dagger \mathcal{H} U - i U^\dagger \frac{dU}{dz}. \quad (\text{S20})$$

Define $\phi(z) \equiv m_a z + \varphi_a$, the photon sub-sector of \mathcal{H} can be decomposed using Pauli matrices:

$$\mathcal{H}_\gamma(z) = -\Delta_\gamma \mathbb{I}_2 - \delta\Delta_\gamma \sigma_z - \Delta_{\text{DM}} \sin \phi \sigma_y, \quad (\text{S21})$$

where $\Delta_\gamma = (\Delta_\perp + \Delta_\parallel)/2$ and $\delta\Delta_\gamma = (\Delta_\perp - \Delta_\parallel)/2$. We introduce a time-dependent unitary rotation acting in the photon subspace

$$u(z) = \exp[-i\theta(z)\sigma_y], \quad \theta(z) = \alpha \cos \phi(z). \quad (\text{S22})$$

The transformation matrix is

$$U(z) = \begin{pmatrix} \cos \theta & -\sin \theta & 0 \\ \sin \theta & \cos \theta & 0 \\ 0 & 0 & 1 \end{pmatrix}. \quad (\text{S23})$$

The term $iu^\dagger \partial_z u$ can be calculated as

$$iu^\dagger \partial_z u = -\alpha m_a \sin \phi u^\dagger \sigma_y u = -\alpha m_a \sin \phi \sigma_y, \quad (\text{S24})$$

where the final step utilises the fact that σ_y commutes with itself. To cancel the $-\Delta_{\text{DM}} \sin \phi \sigma_y$ term in the Hamiltonian, we set $\alpha = \Delta_{\text{DM}}/m_a$, yielding the effective Hamiltonian

$$\mathcal{H}'(z) = - \begin{pmatrix} \Delta_\gamma + \delta\Delta_\gamma \cos(2\theta) & \delta\Delta_\gamma \sin(2\theta) & \Delta_B \sin \theta \\ \delta\Delta_\gamma \sin(2\theta) & \Delta_\gamma - \delta\Delta_\gamma \cos(2\theta) & \Delta_B \cos \theta \\ \Delta_B \sin \theta & \Delta_B \cos \theta & \Delta_a \end{pmatrix}. \quad (\text{S25})$$

When $|\delta\Delta_\gamma| \ll m_a$ and Δ_{DM} , the phase evolution rate due to QED birefringence becomes negligible compared to the DM modulation frequency. In this regime, the photon states are effectively degenerate for axions, allowing the QED contribution to be safely neglected. The transformed Hamiltonian simplifies to

$$\mathcal{H}'(z) = - \begin{pmatrix} \Delta_\gamma & 0 & \Delta_B \sin \theta \\ 0 & \Delta_\gamma & \Delta_B \cos \theta \\ \Delta_B \sin \theta & \Delta_B \cos \theta & \Delta_a \end{pmatrix}. \quad (\text{S26})$$

For $\Delta_B \ll |\Delta_\gamma - \Delta_a|$, the dynamics can be analyzed by treating each photon mode-axion pair independently under the rotating-wave approximation. The two-state systems are governed by couplings $G^{(1)} = \Delta_B \sin \theta$ and $G^{(2)} = \Delta_B \cos \theta$. Expressing $\sin \theta$ and $\cos \theta$ via the Jacobi–Anger identity

$$e^{i\alpha \cos \phi} = \sum_{\ell=-\infty}^{\infty} i^\ell J_\ell(\alpha) e^{i\ell\phi}, \quad (\text{S27})$$

we expand $G^{(1,2)}$ into Fourier harmonics:

$$G^{(1)}(z) = \frac{\Delta_B}{2i} \sum_{\ell} [1 - (-1)^\ell] i^\ell J_\ell(\alpha) e^{i\ell\phi}, \quad (\text{S28})$$

$$G^{(2)}(z) = \frac{\Delta_B}{2} \sum_{\ell} [1 + (-1)^\ell] i^\ell J_\ell(\alpha) e^{i\ell\phi}. \quad (\text{S29})$$

Thus, each photon mode couples to the axion through a series of sidebands with frequencies ℓm_a . $G^{(1)}$ and $G^{(2)}$ carry odd and even harmonics, respectively. We define the relevant coupling as

$$G(z) = \sum_{\ell \in \mathbb{Z}} g_{\ell\ell} e^{i\ell m_a z}, \quad (\text{S30})$$

with

$$g_\ell^{(1)} = \frac{[1 - (-1)^\ell] i^{\ell-1} e^{i\ell\varphi_a}}{2} J_\ell(\alpha) \Delta_B, \quad (\text{S31})$$

$$g_\ell^{(2)} = \frac{[1 + (-1)^\ell] i^\ell e^{i\ell\varphi_a}}{2} J_\ell(\alpha) \Delta_B. \quad (\text{S32})$$

Focusing on a single photon mode, the coupled equations become:

$$-i \frac{d}{dz} \Phi_\gamma = \Delta_\gamma \Phi_\gamma + G(z) \Phi_a, \quad (\text{S33})$$

$$-i \frac{d}{dz} \Phi_a = G(z) \Phi_\gamma + \Delta_a \Phi_a. \quad (\text{S34})$$

Moving to the interaction picture via $\Phi_\gamma = \tilde{\Phi}_\gamma e^{i\Delta_\gamma z}$, $\Phi_a = \tilde{\Phi}_a e^{i\Delta_a z}$, we obtain

$$-i \frac{d}{dz} \tilde{\Phi}_\gamma = \sum_\ell g_\ell e^{-i\delta_\ell z} \tilde{\Phi}_a, \quad (\text{S35})$$

$$-i \frac{d}{dz} \tilde{\Phi}_a = \sum_\ell g_\ell^* e^{i\delta_\ell z} \tilde{\Phi}_\gamma, \quad (\text{S36})$$

with

$$\delta_\ell = \Delta_\gamma - \Delta_a - \ell m_a. \quad (\text{S37})$$

Resonance occurs when the phase oscillation is slow, i.e., when the momentum mismatch is compensated by the axion mass harmonics. Retaining the resonant harmonic $\ell = n$ that satisfies $\delta_n \approx 0$, we obtain the Rabi oscillation dynamics with an effective Rabi frequency

$$\Omega_R = \sqrt{|g_n|^2 + (\delta_n/2)^2}. \quad (\text{S38})$$

The conversion probability is given by:

$$P_{\gamma \rightarrow a} = \frac{|g_n|^2}{\Omega_R^2} \sin^2(\Omega_R z). \quad (\text{S39})$$

Additionally, we discuss the choice of transformations for diagonalizing the Hamiltonian \mathcal{H} . In general, Floquet theory can be directly applied to the three-level system. However, to isolate the dominant resonant dynamics and obtain a transparent physical picture, we diagonalize the photon subspace and reduce the problem to effective two-level photon–axion systems. An intuitive choice is to transform to the circular polarization basis using

$$U_C(z) = \frac{1}{\sqrt{2}} \begin{pmatrix} 1 & i & 0 \\ 1 & -i & 0 \\ 0 & 0 & 1 \end{pmatrix}. \quad (\text{S40})$$

The Hamiltonian is given by

$$\mathcal{H}'_C = - \begin{pmatrix} \Delta_+ & \delta\Delta_\gamma & \frac{\Delta_B}{\sqrt{2}} \\ \delta\Delta_\gamma & \Delta_- & \frac{i\Delta_B}{\sqrt{2}} \\ \frac{\Delta_B}{\sqrt{2}} & -\frac{i\Delta_B}{\sqrt{2}} & \Delta_a \end{pmatrix} \quad (\text{S41})$$

where $\Delta_\pm = \Delta_\gamma \mp \Delta_{\text{DM}} \sin \phi$ represent the photon dispersion for the two circular polarizations. Neglecting the QED birefringence effect, the evolution for the photon state can be formally written as

$$\Phi_\pm \simeq \exp \left[-i \int^z dz' (\Delta_\gamma \mp \Delta_{\text{DM}} \sin \phi(z')) \right] \tilde{\Phi}_\pm \quad (\text{S42})$$

$$= e^{-i\Delta_\gamma z} e^{\pm i\alpha \cos \phi} \tilde{\Phi}_\pm. \quad (\text{S43})$$

Repeating the Fourier harmonic expansion as above, one would also obtain the same resonance condition and Rabi oscillations. It has been noted that coherent axion background induces a periodic frequency modulation of photon propagation in Ref. [40]. However, in that work the modulation is treated as a phase modulation of a fixed propagation eigenmode, and physical observables are obtained after averaging over the axion oscillation. As a result, the associated sidebands are not promoted to independent dynamical degrees of freedom. This procedure effectively restricts the dynamics to a single Floquet sector and is equivalent to replacing the time-ordered evolution operator by one generated by an averaged Hamiltonian. Such treatments effectively average over the harmonic structure of the modulation and therefore do not capture the Floquet sidebands responsible for resonant mode mixing.

The transformations $U(z)$ and U_C offer two distinct yet complementary physical interpretations. The transformation $U(z)$ represents a co-rotating frame perspective. By shifting into a basis that rotates alongside the axion-induced birefringence effect, we effectively eliminate the rapid oscillations of the off-diagonal mixing terms. In this frame, the interaction is understood through the lens of geometric phase, where the coupling to the axion arises from the mismatch between the photon's polarization drift and the background field's oscillation frequency.

The circular basis U_C provides a frequency modulation perspective. Here, the axion field acts as a dynamic medium that oscillates the refractive indices of the left- and right-handed circular polarizations in opposite phases. The resonance condition is explained by the Jacobi-Anger expansion, where the carrier frequency of the photon acquires sidebands at integer multiples of the axion mass m_a . While both methods yield identical Rabi frequencies for the resonant transition, the circular basis is often more robust when incorporating higher-order corrections, such as QED birefringence, as it treats the two helicity states as the fundamental vacuum eigenmodes.

COHERENT MODE MIXING VS. PARAMETRIC INSTABILITY

In the literature on axion electrodynamics, it is well established that an oscillating axion background can induce a parametric instability in the electromagnetic field. This is often formulated using the Mathieu equation and interpreted as the stimulated decay of axions into photons. Superficially, this resembles the propagation equation, Eq. (S12), utilized in this work, where the mixing matrix $\mathcal{M}(z)$ also contains a periodic contribution from the axion DM background. In this appendix, we clarify that these two phenomena, despite originating from the same Lagrangian, describe physically distinct regimes and yield qualitatively different results.

Common Origin

Both formalisms derive from the standard axion–photon Lagrangian Eq. (S1). Consider a classical, coherently oscillating axion background

$$a(t) \sim a_0 \cos(m_a t). \quad (\text{S44})$$

Maxwell's equations acquire an explicit time dependence, characterized by Eqs. (S6) to (S8). However, the subsequent reduction of these equations depends critically on the physical boundary conditions and the kinematic regime of interest.

Regime I: Parametric Instability (The Mathieu Limit)

The analysis of axion-induced parametric instability typically focuses on the spontaneous production and amplification of photon modes from the vacuum (or a low-occupation state). In this regime, one must retain the full second-order time dynamics, including both positive- and negative-frequency components of the field momentum modes:

$$\mathbf{A}(\mathbf{x}, t) \sim A_{\pm}(t) e^{i\mathbf{k} \cdot \mathbf{x}}, \quad A_{\pm}(t) = c(t) e^{-i\omega t} + c^*(t) e^{+i\omega t}. \quad (\text{S45})$$

For circular polarizations, the equation of motion reduces to a Mathieu equation:

$$\ddot{A}_{\pm} + \omega^2 [1 \pm \epsilon \cos(m_a t)] A_{\pm} = 0, \quad (\text{S46})$$

where $\epsilon \sim g_{a\gamma} a_0 m_a / \omega$. The defining feature of this regime is that the periodic axion background modulates the effective frequency squared of the oscillator. This modulation couples the positive-frequency ($e^{-i\omega t}$) and negative-frequency ($e^{+i\omega t}$) modes. When $m_a \simeq 2\omega$, the system enters an instability band where the field amplitude grows exponentially.¹ This corresponds to the stimulated decay of the axion field into photon pairs, a genuine parametric instability where the background acts as an energy pump.

¹ The instability of the photon–axion system—considering both axion DM and magnetic fields but omitting the plasma back-

ground—is explored in Ref. [39], where an instability condition $\sqrt{k_{\gamma}^2 + m_a^2} + k_{\gamma} = nm_a$ is identified.

Regime II: Coherent Mode Mixing (The Propagation Limit)

In contrast, this work investigates the propagation of a pre-existing electromagnetic wave with a fixed carrier frequency ω and well-defined direction. Employing the slowly varying envelope approximation, we express the field as a slowly evolving amplitude modulating a rapid oscillatory phase. Crucially, this procedure effectively integrates out backward-propagating and negative-frequency modes. The resulting dynamics are governed by Eq. (S12). While the axion background still introduces a periodic modulation in the mixing matrix $\mathcal{M}(z)$, its physical role changes fundamentally:

- The modulation acts as a linear, Hermitian coupling between forward-propagating modes (e.g., photon polarization states).
- It does *not* couple positive- and negative-frequency solutions.

Consequently, the system does not exhibit Mathieu-type exponential instabilities. Instead, it displays Floquet resonances—enhanced but bounded mode conversion—when the eigenvalue difference matches the modulation frequency: $\lambda_i - \lambda_j = nm_a$.

Theoretical Synthesis

The distinction between these two phenomena can be understood by analogy to quantum optical systems.

Parametric Instability (Regime I) is analogous to a driven harmonic oscillator. A periodic modulation of the oscillator’s parameters leads to exponential growth of the mode amplitude within instability bands. In quantum terms, this represents parametric amplification, or particle creation from the vacuum.

Floquet Mixing (Regime II) is analogous to a driven multi-level system, such as Rabi oscillations in atomic physics. The relevant degrees of freedom are discrete internal states, and the periodic background induces transitions among them. Probabilities oscillate but remain bounded (unitary evolution).

From a formal Floquet theory perspective, both systems involve linear differential equations with periodic coefficients. However, the spectral implications differ:

- In the Mathieu case (Instability), the Floquet quasi-energies can acquire imaginary parts, signaling an unbounded instability.
- In the Propagation case (Mixing), the quasi-energies remain real. Resonances here correspond to avoided crossings in the quasi-energy spectrum, maximizing the mixing angle between states rather than the total energy of the system.

Thus, while both phenomena arise within the framework of periodically driven systems, the propagation formalism employed in this work isolates the physics of coherent state mixing, explicitly distinct from the particle-production physics of parametric instability.

NUMERICAL ANALYSIS

To numerically verify the analytical framework, we solve the Eq. (S16) incorporating the mixing matrix \mathcal{M} for a concrete astrophysical environment. We model the relativistic jet of blazar 3C 279, focusing on the unpolarized optical R-band photons ($E_\gamma \approx 1.9$ eV) with a representative parameter set: an axion mass $m_a = 10^{-22}$ eV and a coupling constant $g_{a\gamma} = 5 \times 10^{-11}$ GeV $^{-1}$. The radiation zone, located $r_0 = 0.5$ pc from the central engine, is characterized by a magnetic field $B_0 = 0.5$ G and electron density $n_{e,0} = 5 \times 10^3$ cm $^{-3}$ [45]. The jet is modeled as a conical outflow with a Doppler factor $\delta \simeq 13$ [45], assuming scaling profiles $B(r) \propto r^{-1}$ and $n_e(r) \propto r^{-2}$ over a total length $L_{\text{jet}} = 1$ kpc. To capture the fine-grained evolution of the mixing process, the calculation is performed over domain sizes ranging from 5×10^{-7} pc to 10^{-3} pc.

To isolate and illustrate the resonance structures dictated by the plasma profile, we adopt a uniform DM density $\rho_{\text{DM}} = 1$ GeV \cdot cm $^{-3}$ ($2.63 \times 10^7 M_\odot \cdot \text{kpc}^{-3}$), and obtain the photon–axion conversion probability shown in Fig. 1. Fig. 1 demonstrates resonant conversion exactly at the locations predicted by Eq. (11), while the behavior reduces

to the adiabatic limit away from resonance. This excellent agreement confirms that the Floquet analysis accurately describes the physics of the driven system. The conversion probability exhibits a distinct step-like growth, indicating that resonant conversion occurs within narrow spatial windows where the phase-matching condition is satisfied. The resonance positions depend solely on the jet's plasma profile and the axion mass, independent of the DM density ρ_{DM} . Thus, while a realistic non-uniform DM halo would modulate the amplitude of each "step" according to local ρ_{DM} and B values, the qualitative structure of multiple resonances remains unchanged.

The spatial width of the Floquet resonance L_{res} can be estimated as $|4g_n/(\nabla_r \delta_n)|_{r_{\text{res}}}$. For the jet model considered here, the resonance width is approximately $2(nm_a)^{-1} g_{a\gamma} B_0 J_n(\alpha) r_0$. For the parameters used in Fig. 1, we obtain $L_{\text{res}} \sim 3 \text{ pc}$, in agreement with the numerical results. This finite width confirms that the resonance is robust against density fluctuations on scales smaller than L_{res} . Given that L_{res} is two orders of magnitude smaller than the total jet length ($\sim \text{kpc}$), plasma density variations within each resonance region are negligible. This separation of scales ensures that the resonance remains robust even in highly inhomogeneous jet environments, where the global density gradient merely serves to sequentially satisfy discrete resonance conditions.

The Floquet resonance relies on the coherent oscillation of the axion field. The validity of this assumption depends on the coherence time of the DM field, $\tau_{\text{coh}} \sim (m_a v^2)^{-1}$, compared to the photon's transit time through the resonance region, $t_{\text{cross}} \sim L_{\text{res}}$. For ultralight axions considered here with virial velocity $v \sim 10^{-3}$, the coherence time is $\tau_{\text{coh}} \sim \mathcal{O}(10^5)$ years. In contrast, the spatial width $L_{\text{res}} \sim 3 \text{ pc}$ corresponds to a transit time $t_{\text{cross}} \approx 10$ years. The condition $t_{\text{cross}} \ll \tau_{\text{coh}}$ ensures that the DM background acts as a highly coherent driving force during the resonant interaction. Moreover, the fractional frequency spread $\delta m_a/m_a \sim 10^{-6}$ induces a negligible broadening of the resonance layer compared to its physical width determined by the jet geometry and coupling strength.

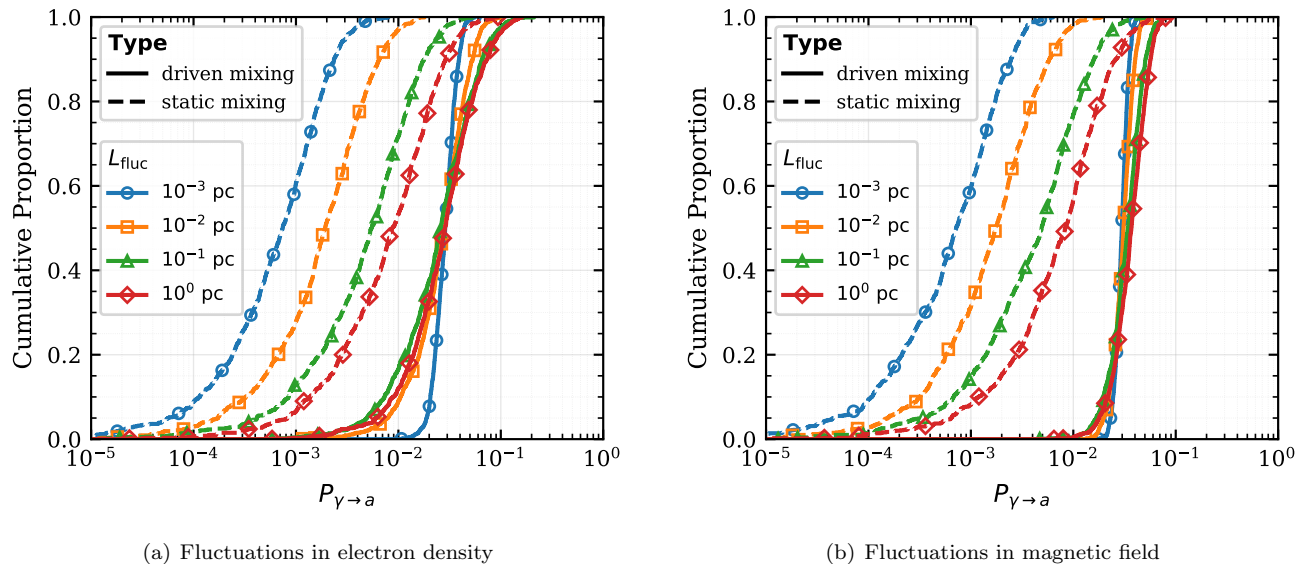


Figure S1. Empirical cumulative distribution function (ECDF) of the photon-to-axion conversion probability $P_{\gamma \rightarrow a}$. The colors represent different fluctuation correlation lengths L_{fluc} , ranging from 10^{-3} to 1 pc. Panels (a) and (b) correspond to stochastic fluctuations in the electron density and magnetic field, respectively. Solid and dashed lines distinguish between driven Floquet mixing with oscillating DM background and adiabatic conversion with static DM background. Each curve is generated from $N = 1000$ random realizations. Note that the x -axis is on a logarithmic scale.

The phenomenological impact of this mechanism depends on the degree to which phase coherence is maintained along the propagation path. Strong gradients or rapid environmental variations can disrupt the driven mixing and suppress the resonance, while sufficiently smooth backgrounds allow the periodically driven dynamics to operate effectively. In such regimes, the driven contribution to photon-axion mixing can be comparable to, or exceed, that expected from static conversion alone.

To assess the robustness of the resonance mechanism, we investigate the effects of stochastic fluctuations in the electron density and the magnetic field separately. The propagation path is partitioned into discrete domains of length L_{fluc} . For each scenario, we introduce a random bias by scaling the baseline model value by a coefficient ξ , uniformly sampled from $[0.5, 1.5]$, thereby representing 50% amplitude fluctuations. As shown in Fig. S1, even with these 50% amplitude variations, the mean conversion probability under Floquet-driven mixing remains consistently

1–2 orders of magnitude higher than in the standard static scenario across all considered correlation lengths. While small-scale fluctuations ($L_{\text{fluc}} \ll L_{\text{res}}$) are effectively self-averaged, larger-scale variations ($L_{\text{fluc}} \sim 1$ pc) increase statistical variance by inducing local dephasing. Nevertheless, the empirical cumulative distribution function (ECDF) reveals that even the lower quantiles of these distributions significantly surpass the standard adiabatic case.

This resilience stems from the "hard-driving" nature of the Floquet resonance, where the global coherence of the axion oscillation frequency m_a exerts a persistent periodic force that facilitates mode-mixing despite environmental noise. Even when the resonance condition is fragmented by medium-scale turbulence, the collective accumulation of these imperfect resonances ensures a statistically robust conversion probability.

Standard astrophysical emission mechanisms in blazars typically yield negligible circular polarization. However, the Floquet resonance breaks the degeneracy between left- and right-handed circular polarization states through the parity-violating coupling. This induces a non-zero net circular polarization, whose sign and magnitude are stochastic and depend on the phase φ_a of the axion background at the resonance onset.

This stochastic circular polarization arises from coherent, unitary mode mixing and is therefore qualitatively distinct from polarization generated by absorption or scattering processes. The magnitude of the variance is directly controlled by the resonance strength, thereby providing a direct probe of the driven mixing mechanism. Importantly, this polarization signature does not rely on fine-tuned source properties or detailed environmental modeling. It follows directly from the existence of Floquet resonances in photon propagation through a coherent axion background.

We apply the formalism to constrain the axion–photon coupling $g_{a\gamma}$ using optical polarimetry of 3C 279. The DM density is modeled using a fuzzy DM profile, which consists of a solitonic core and an outer NFW envelope [46, 47] with the total mass $M_h \sim 10^{13} M_\odot$ [48]. The core density profile is adopted as $\rho_c [1 + 0.091(r/r_c)^2]^{-8}$ with the core radius $r_c \simeq 1.6$ kpc $(m/10^{-22} \text{ eV})^{-1} (M_h/10^9 M_\odot)^{-1/3}$ and density $\rho_c \simeq 2.9 \times 10^6 M_\odot \text{ kpc}^{-3} (m/10^{-22} \text{ eV})^2 (M_h/10^9 M_\odot)^{4/3}$ [49]. The transition radius between the two regions is taken to be $r_t \simeq 3r_c$. The concentration parameter of the NFW halo is determined using the concentration–mass relation at redshift $z = 0.5$ [50]. This configuration yields negligible spatial gradients with $\mathcal{F} \lesssim 10^{-3}$.

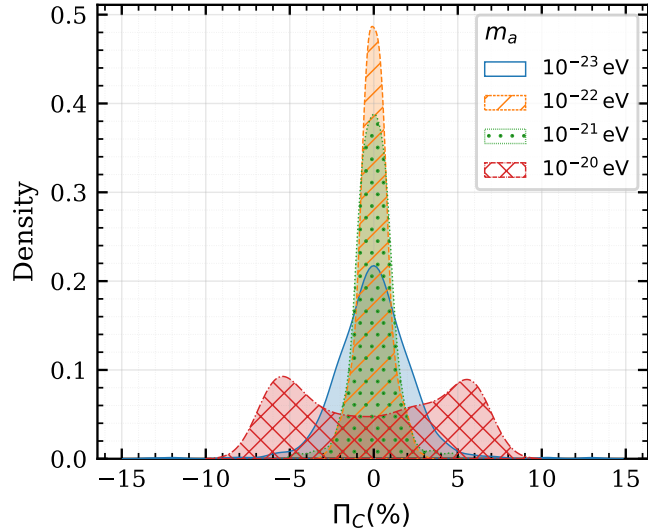


Figure S2. Probability density of induced circular polarization for various axion masses m_a (assuming $g_{a\gamma} = 5 \times 10^{-11} \text{ GeV}^{-1}$), estimated via Kernel Density Estimation (KDE) by uniformly sampling the axion phase $\varphi_a \in [0, 2\pi]$. The shaded profiles are generated using Gaussian kernels with Scott's rule bandwidths. The transition from single-peaked to double-peaked distributions illustrates the varying sensitivity of the conversion process to the axion phase across different mass regimes.

For each parameter pair $(m_a, g_{a\gamma})$, we solved the equations of motion 1,000 times, using equally spaced values between 0 and 2π for the axion phase φ_a and assuming a 30% initial linear polarization [43], then we obtained a well-resolved ensemble of induced circular polarization. In Fig. S2, the resulting probability density of the degree of circular polarization Π_C is visualized using the kernel density estimation.

To derive constraints on the axion–photon coupling $g_{a\gamma}$, we adopt a source-agnostic statistical criterion: the standard deviation of the axion-induced circular polarization σ_{std} must not exceed the characteristic observational uncertainty of a given source. For the case of 3C 279, we take $\sigma_{\Pi_C} \approx 0.30\%$ [43]. This criterion ensures consistency between the

predicted stochastic signal and the measured noise level without assuming a deterministic phase alignment. For any astrophysical source, the axion phase φ_a is effectively constant over observational timescales. However, since its value is a priori unknown, the axion-induced circular polarization manifests as a stochastic contribution with vanishing mean. Even when the axion-induced circular polarization exhibits a bimodal distribution for certain masses, its sign and magnitude remain observationally unpredictable due to the unknown axion phase, making the variance a physically meaningful measure of its impact. Requiring its variance not to exceed the instrumental sensitivity therefore provides a consistency bound that is insensitive to detailed phase realizations. Figure 2 shows the resulting illustrative bound in parameter space, with CAST limits [44] included for scale comparison.

For $m_a \in [10^{-23}, 10^{-20}]$ eV, this procedure yields limits at the level of $g_{a\gamma} \lesssim 2 \times 10^{-11}$ GeV $^{-1}$. The distinctive band-like structure of the resulting contour is a characteristic fingerprint of the Floquet-driven mode mixing mechanism, requiring driven, time-dependent mixing and the associated discrete resonance structure. Two generic features emerge from this mechanism: (1) The conversion efficiency, affected by the Bessel functions $J_n(\Delta_{\text{DM}}/m_a)$, is maximized when the effective momentum mismatch is bridged by integer harmonics of m_a , a direct consequence of the periodic Floquet driving. The sharp dips in the consistency bound correspond to resonance “sweet spots” where this condition is optimally satisfied, largely independent of the detailed jet profile. (2) As m_a varies, the dominant contribution shifts discretely between different resonance orders n , producing the characteristic banded pattern. Weaker constraints between bands reflect off-resonance regimes, where the system approaches the adiabatic limit and the driven mixing becomes inefficient, resulting in suppressed circular polarization production.

Although the current limit region is normalized to the specific noise floor of 3C 279, the qualitative structure of the constraint reflects a phenomenological consequence of the underlying mechanism, thereby illustrating the physical relevance of the framework.